Catalysis Today 138 (2008) 203–209

Contents lists available at ScienceDirect

Catalysis Today

journal homepage: www.elsevier.com/locate/cattod

# In situ hydrogen generation from cycloalkanes using a Pt/CNF catalyst

M.P. Lázaro, E. García-Bordejé *, D. Sebastián, M.J. Lázaro, R. Moliner

*Instituto de Carboquímica (C.S.I.C.), Miguel Luesma Castán 4, 50018 Zaragoza, Spain*

ARTICLE INFO

*Article history:*
Available online 24 June 2008

*Keywords:*
Pt catalyst
Carbon nanofibers
Hydrogen production
Decalin

ABSTRACT

Pt catalyst supported on carbon nanofibers (CNFs) has been prepared via ion-exchange and it was characterized by XRD, TEM, $N_2$ physisorption and CO chemisorption. The Pt/CNF catalyst has a small Pt crystallite size in the range of 2–3 nm. This catalyst has been tested in the dehydrogenation of decalin, which is a cycloalkane proposed in the literature as $H_2$ storage media for vehicles and portable devices. The objective is finding a Pt catalyst suitable for in situ generation of $H_2$ from chemical storage in decalin. The results revealed that Pt supported on CNF outperforms a Pt catalyst supported on micro–mesoporous activated carbon. Finally, we propose a reactor configuration aiming at the intensification of $H_2$ production in continuous.



## 1. Introduction

One of the main hurdles for the implementation of "Hydrogen economy" is the storage and delivery of $H_2$ for automotive vehicles. Regarding the storage system, the DOE has set the objective of 9 wt.% for 2015 including the vessel. This target has prompted the search for storage media alternative to the classical high-pressure tanks and insulated liquid-hydrogen systems. Polymer electrolyte membrane (PEM) fuel cells will be the fuel cell of choice for vehicles because it operates at low temperature (<100 °C). Low temperature operation is preferable when fast start-up and shut down is needed, as occurs in cars. Normally, PEM have to be fed with hydrogen containing less than ~5 ppm CO to avoid poisoning of Pt in the cathode.

There are several options under investigation to store and release hydrogen on demand in a car. It is convenient to carry out $H_2$ generation at low temperature for improved transient kinetics and energy economy. Currently, most of the methods for producing hydrogen operate at high reaction temperature. For instance, the most popular method of steam methane reforming requires reaction temperatures >700 °C. Due to economical and social reasons, it is also desirable that $H_2$ carrier could be delivered using infrastructures of the conventional fuels. From this standpoint, the $H_2$ chemical storage in liquid compounds must be the best option.

The so-called "organic hydrides" are liquid cycloalkanes that can use the current delivery infrastructures. Dehydrogenation of cycloalkanes has been well documented for seasonal storage of energy through storage and supply of hydrogen [1,2]. Among cycloalkanes, cyclohexane [3,4], methyl cyclohexane [5] and decalin [6–8] are the most studied. As model compound of "organic hydrides", we have chosen decalin, which has a storage density of 7.3 wt.%, and 64.8 kg-$H_2$/m$^3$, exceeding those of conventional storage media such as compressed or cryogenic $H_2$. Decalin has the following advantages: (i) evaporation loss during storage is negligible because of the high boiling points (*cis*-decalin, 187 °C; *trans*-decalin, 196 °C; tetraline, 207 °C, naphthalene 218 °C); (ii) the dehydrogenation energy of decalin is 10–13 kcal/mol, which allows performing the dehydrogenation at low temperatures (<200 °C); (iii) it has low toxicity and environmental impact; (iv) there are no parallel reactions enabling multiple cycles without degradation; (v) it has low cost since it is prepared from natural raw materials. Recently, Froment and co-workers [9] have proposed decalin as a serious candidate for $H_2$ storage because it yields pure $H_2$ and the catalyst deactivation is slow. Recently, also other potential "organic hydrides" with higher $H_2$ densities and lower dehydrogenation enthalpies have been described based on theoretical predictions [10].

In order to generate $H_2$ in situ, it is necessary to have a system which is able to release $H_2$ from the chemical compound. This can be accomplished by the use of a catalytic reactor that dehydrogenates the organic "hydride" on board. This reactor can be integrated in a car as illustrated in Fig. 1. Likewise, the waste heat of fuel cell could sustain the endothermic dehydrogenation.

Both monometallic (Pt, Pd, Ru, and Pt) [11] and bimetallic (Pt with Ni, Pt, Pd, Rh or Ir) [3,5,11–13] catalysts have been used for this reaction. Activated carbon is the support used commonly for cycloalkane dehydrogenation because of its inertness for catalysing side reactions. The use of carbon nanofibers (CNFs) or carbon

* Corresponding author. Tel.: +34 976733977; fax: +34 976733318.
*E-mail address:* jegarcia@carbon.icb.csic.es (E. García-Bordejé).

0920-5861/$ – see front matter © 2008 Elsevier B.V. All rights reserved.
doi:10.1016/j.cattod.2008.05.011

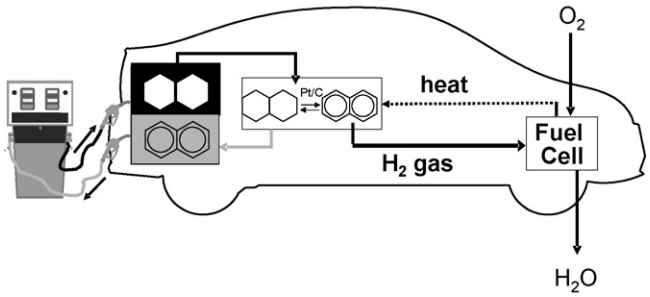


**Fig. 1.** Scheme of a fuel cell-driven vehicle that is fed with $H_2$ supplied by decalin dehydrogenation.

nanotubes (CNTs) as catalyst support has been applied scarcely to this reaction [14,15]. These authors claim that a 0.25 wt.%/CNF catalyst shows the same activity and selectivity than a commercial 1 wt.% $Pt/Al_2O_3$ for the dehydrogenation of cyclohexane. They attribute this to a better dispersion of Pt. Contrarily to microporous activated carbons, the open structure of CNF/CNT without microporosity may favour the accessibility of the liquid reactant to the catalytic sites and desorption of the liquid products.

Herein, we have prepared a catalyst consisting of Pt supported on CNFs and we have tested this catalyst in the dehydrogenation of decalin in a batch reactor. In this work, we study the influence of decalin/catalyst ratio. In addition, we compare the results of Pt/CNF catalyst with our previous results with a catalyst of Pt supported on a micro–mesoporous activated carbon. Finally, bearing in mind the intensification of the process, we propose a catalytic reactor for the dehydrogenation in continuous on board of a vehicle.

## 2. Experimental

Carbon nanofibers were grown via $CH_4$ decomposition over a Ni:Cu:Al catalyst prepared by co-precipitation as described previously [16]. Briefly, first the catalyst was reduced during 3 h in $H_2$ flow at 550 °C. Subsequently, the CNFs were grown at 973 K by flowing 20 ml/min of $CH_4$ during 8 h. The as-grown CNFs were oxidised with concentrated $HNO_3$ during 0.5 h under boiling and reflux conditions. The oxidation is carried out for two reasons, namely, for removing growth catalyst and for creating oxygenated surface groups.

Pt was deposited on the oxidised CNFs from an aqueous solution of $Pt(NH_3)_4Cl_2$ by ion-exchange of the cationic precursor with the protons of the CNF oxygenated functional groups. In brief, 0.1 g of $Pt(NH_3)_4Cl_2$ was dissolved in 60 ml of $H_2O$. Subsequently, 1 g of CNF was added to the solution and the pH of the slurry was adjusted to 9 by adding a few $NH_3$ droplets (25%). The slurry was kept under stirring overnight. Finally, the catalyst was filtered, dried, calcined at 623 K in $N_2$ and reduced in a 50% $H_2$:$N_2$ mixture at 623 K. Both calcination and reduction were conducted with a heating ramp of 3 °C/min and a dwell time of 2 h. The Pt uptake in the CNF was calculated from the difference of Pt concentration between the initial and final solutions measured by ICP-OES. The catalyst supported on activated carbon (Pt/AC) was prepared by adsorption of $H_2PtCl_6$ on a mesoporous activated carbon (Engelhard italiana S.p.A) as described previously [17].

The catalysts were characterized by XRD, TEM, $N_2$ physisorption and CO chemisorption. XRD patterns were recorded using a Bruker AXS D8ADVANCE diffractometer, in a $\theta$–$\theta$ configuration and with a nickel-filtered Cu K$\alpha$ radiation. Nitrogen adsorption–desorption isotherms were measured at 77 K using a Micromeritics ASAP 2020. Total surface area and pore volumes were determined using the BET (Brunauer–Emmett–Teller) equation and the single point method, respectively. Mesopore volume was determined by *t*-plot method. TEM images of Pt/CNF were obtained using a 300 kV Philips CM-30 TEM. For such measurements, the samples were suspended in ethanol with ultrasonic dispersion. Later, they were deposited on a holey carbon grid and, after drying, the grid was ready for observation. Pulse CO chemisorption tests were performed in a Micromeritics AutoChemII 2920. The catalyst samples were pre-reduced in a 30 ml/min flow of $H_2$ at 110 °C for 1 h. The samples were cooled down to 45 °C, and the 0.5 $cm^3$ pulses of a mixture of 10% CO in Ar were supplied to the samples until saturation of CO was reached. The amounts of CO chemisorbed were calculated from the data obtained from the pulse CO chemisorption tests.

Finally, the catalysts were tested in the dehydrogenation of decalin in the temperature range 493–533 K in a batch glass reactor (Fig. 2) as that described previously [17]. The void volume of the reactor below the condenser is 90 $cm^3$. In a standard experiment, 0.3 g of catalyst is loaded forming a thin layer at the bottom of the reactor vessel. A known amount of decalin (Fluka, reagent grade) is added to the catalyst dropwise to ensure that all the catalyst is wetted with decalin. The volumes of decalin used were 0.3, 0.6, 0.8, 1 and 1.5 ml giving rise to different decalin/catalyst ratios. Then the experimental set-up is mounted and the reactor volume is swept with $N_2$ during 15–20 min to purge all $O_2$ remaining inside the system. In parallel, a molten salts bath (equimolar $KNO_3$–$NaNO_3$) is heated to the reaction temperature. When the bath temperature reaches the set value, the reactor vessel is introduced in the bath and the reaction starts. The water volume displaced in a burette monitored the $H_2$ volume released during the reaction. When the reactor is cooled down after reaction, the catalyst and reactor are washed with *n*-hexane. This *n*-hexane is filtered and analysed by gas chromatography

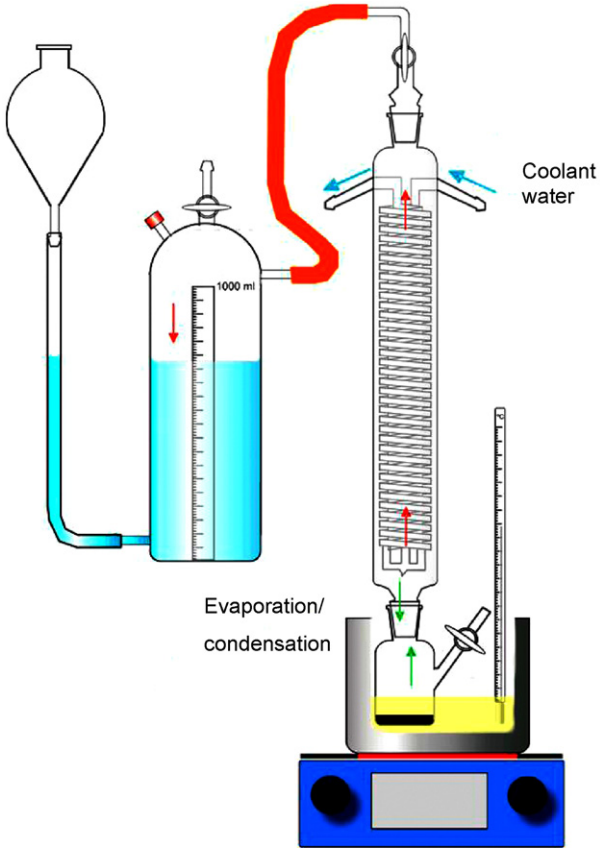


**Fig. 2.** Set up used for decalin dehydrogenation tests in batch operation.

(Hewlett-Packard 5890 series II with selective mass detector). In the chromatographs of all the samples, four peaks were found, which correspond to *trans*-decalin, *cis*-decalin, tetralin (very low intensity) and naphthalene, in increasing order of retention times. A material balance to the final concentration of liquid reactant and products confirmed the decalin conversion calculated from evolved $H_2$. In our experiments, we call reaction temperature to that in the heating bath, which must be approximately the same as in the catalyst surface at the bottom of the reactor vessel.

## 3. Results and discussion

### 3.1. Thermodynamic considerations of decalin dehydrogenation

Fig. 3a shows the theoretical thermodynamic equilibrium compositions vs. reaction temperature in gas phase. Equilibrium compositions were calculated using the software HSC chemistry (Outotec). This commercial software uses the Gibbs energy minimization method and thermodynamic constants compiled in a database. We assumed that selectivity to tetralin is negligible, i.e. tetralin is readily converted to naphthalene. This assumption is in accordance with our GC analysis and with experiments reported in the literature [9]. The reaction stoichiometry is shown in Eq. (1):

$$\underset{\text{decalin}}{C_{10}H_{18}} \xrightarrow{+\Delta H} [\underset{\text{tetralin}}{C_{10}H_{12}}] + 3H_2 \rightarrow \underset{\text{naphtalene}}{C_{10}H_8} + 5H_2 \quad (1)$$

The decalin feed consisted of 50% *cis*-isomer and 50% *trans*-isomer. Fig. 3a shows that the dehydrogenation of *cis*-decalin predominates over dehydrogenation of *trans*-isomer. Thus, $H_2$ is produced from *cis*-decalin already at 473 K. It is apparent that there is equilibrium between gas and liquid phases. The former phase prevails over the later, which is consistent with an operation temperature above the boiling points of compounds (460 K for *cis*-decalin, 469 K for *trans*-decalin and 491 K for naphthalene).

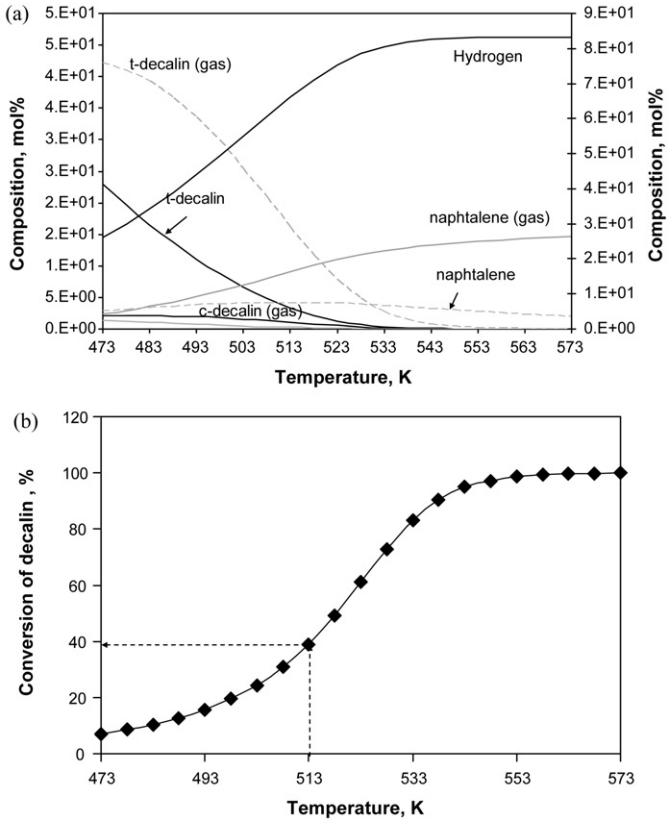


**Fig. 3.** (a) Thermodynamic equilibrium compositions as a function of the temperature calculated using HSC chemistry software. Hydrogen composition corresponds to right *y*-axis. The composition of the rest of compounds is displayed in left *y*-axis. (b) Thermodynamic equilibrium decalin conversion as a function of the temperature calculated using HSC chemistry software.

Fig. 3b shows the calculated decalin conversion. The thermodynamic conversion increases with the temperature, as expected for an endothermic process. The thermodynamic equilibrium predicts 90% decalin conversion at 538 K. For the practical implementation of the catalyst, the goal is performing this reaction at the lowest temperature as possible and with the highest conversion as possible. As a compromise between high conversion and low temperature, we chose 513 K as a standard reaction temperature for the tests. For this temperature, the thermodynamic equilibrium predicts a conversion limit of 40%.

It is important to note that the equilibriums occurring in our experimental set-up are much more complex than equilibrium at a certain temperature. Our system is dynamic with evaporation and condensation of reactants. Furthermore, there is a temperature gradient through the height of our reactor vessel from the top (condenser, ~5 °C) to the bottom where the catalyst is located at the reaction temperature. By doing these thermodynamic calculations we do not aim at simulating the real behaviour of our reactor, which is very complex. We intend just to give an idea of the equilibriums occurring in the ideal case of the whole reactor vessel at isothermal conditions. Nevertheless, the temperature at the thin catalyst layer can be considered constant. Simple calculations indicated that heat involved in all the processes at the catalyst surface (evaporation and reaction) is not significant with respect to the heat supplied by the bath. Furthermore, the heat transport must be fast because the catalyst layer is located at the bottom of reactor vessel, which is in close contact with the heating bath.

### 3.2. Characterization of catalysts

The Pt loading in Pt/CNF measured by ICP-OES amounted to 1.5 wt.%. The Pt loading is determined by the amount of oxygen functional groups amenable for Pt anchorage. Thus, the preparation method of ion-exchange enables to reach only limited Pt loadings. In a previous work [17], we prepared Pt supported on a micro–mesoporous activated carbon, named here as Pt/AC. The Pt/AC catalyst used here has a nominal Pt loading of 3 wt.%. This Pt loading has been chosen because it brought about the best catalytic results after a exhaustive screening of different catalyst loadings [17].

X-ray diffractograms for Pt/CNF and Pt/AC are shown in Fig. 4. As expected, the most visible feature in Pt/CNF is the graphite (0 0 2) diffraction line, located at ~26°. Also discernible are the (1 0 0) and (1 0 1) reflections, which appear in the region between 42° and 45° forming a broad band, and the (0 0 4) line near 55°. We note that the graphite (0 0 2) diffraction line at ~26.3 is very sharp indicating the absence of amorphous carbon. In contrast, Pt/AC exhibits a broad band at 24° and 44°, indicative of amorphous carbon or mixed amorphous/nanocrystalline structure. Pt/CNF also displays the three characteristic peaks for nickel (at $2\theta = 44.5°$ (1 1 1), 51.8° (2 0 0) and 76.4° (2 2 0)). This Ni is due to the residual CNF growth catalyst. The dashed lines indicate the position where platinum reflections should be located. In both catalysts, no reflections due to platinum are observed. This is attributed to the small size of Pt particles (smaller than 3 nm) which is below the detection limit of the apparatus. Confirming the platinum to be present as small nanoparticles been dispersed in both carbon supports.

CO chemisorption results are compiled in Table 1. The Pt dispersion of fresh catalysts is high in both supports giving rise to

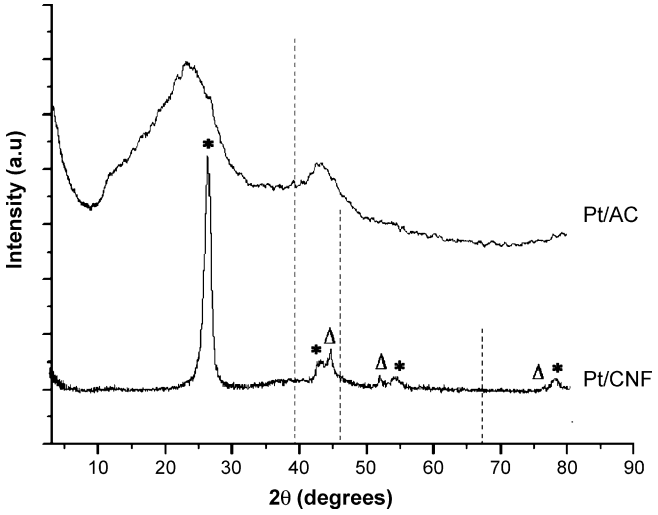


**Fig. 4.** X-ray diffractogramme of Pt/CNF (1.5 wt.% Pt) and Pt/AC (3 wt.% Pt) catalysts. (*) Reflections ascribed to graphite; (Δ) reflections ascribed to nickel. Dashed line indicates where reflections due to platinum should be located.

crystallite sizes of 2.07 nm for Pt/AC and 1.47 nm for Pt/CNF. After reaction, the metallic surface area accessible to CO decreases in both catalyst, more pronouncedly in the case of Pt/AC. This could be due to some sintering but the most probable explanation is that Pt is buried inside plugged micropores as shown in Fig. 8 and Table 2.

Fig. 5 shows a TEM picture representative of the Pt/CNF catalyst. The small dark dots are Pt particles. The inset in the figure displays the particle size distribution, which resulted from the analysis of 100 particles of this sample. It is apparent that 90% of the platinum particles have a particle size lying in the range 2–3.5 nm. TEM analysis gives rise to slightly larger particle size than CO chemisorption. This could be attributed to the fact that the software for image treatment overlooked the smallest Pt particles. Anyway, TEM gives further evidence that the ion-exchange method used here renders well-dispersed and small Pt particles.

CNFs, both as grown and after treatment with $HNO_3$, were burnt in air in a thermobalance. This allowed determining the residual

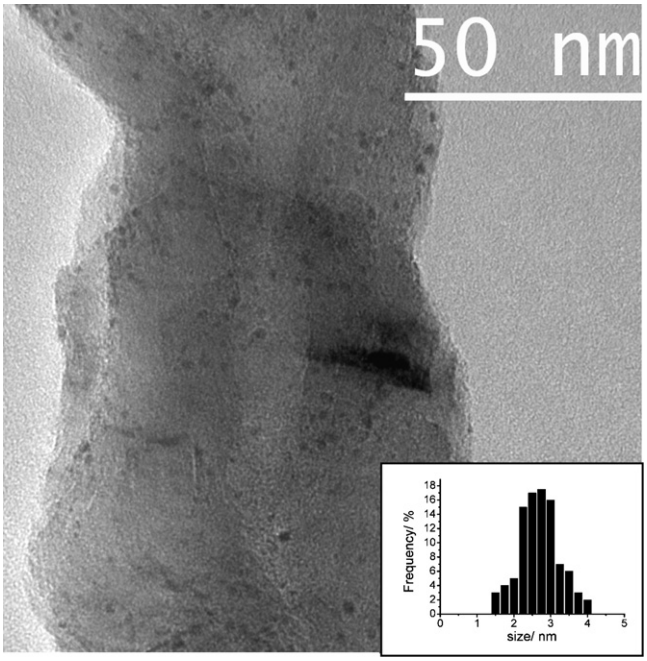


**Fig. 5.** Representative TEM picture of Pt/CNF (1.5 wt.% Pt) catalyst. The inset shows the Pt particle size distribution.

growth catalyst. The as-grown CNFs had a residue of 8 wt.% while the oxidised CNF have a residue of less than 1 wt.%. Thus, after oxidising treatment, most of the growth catalyst is removed. The small remaining residue corresponds to some growth catalyst encapsulated by carbon and therefore it is not active for catalysing any reaction. The inactivity of CNFs used as catalyst support is confirmed below (Fig. 7).

### 3.3. Testing of Pt/CNF in reaction and comparison with Pt/AC performance

Fig. 6 shows the conversion as a function of time-on-stream for tests carried out with Pt/CNF at 513 K with five different decalin/catalyst ratios (ml/g). All experiments exhibit a fast initial increase

**Table 1**
Characterization of catalysts by CO chemisorption

| Catalyst | Pt loading (%) | Condition | CO chemisorption | | |
|---|---|---|---|---|---|
| | | | Dispersion (%)[a] | Metallic surface area $m^2$/g sample | Metal particle diameter (nm)[a] |
| Pt/AC | 3 | Fresh | 54.6 | 6.68 | 2.07 |
| | 3 | After reaction | 37.2 | 4.60 | 3.04[b] |
| Pt/CNF | 1.5 | Fresh | 76.7 | 2.84 | 1.47 |
| | 1.5 | After reaction | 69.8 | 2.58 | 1.62 |

[a] Calculated assuming a stoichiometry factor 1:1.
[b] This is not a real Pt particle size because metallic surface area is not accessible in plugged micropores.

**Table 2**
Textural parameters obtained from $N_2$ adsorption data (77 K)

| Catalyst | Condition | BET area ($m^2$ $g^{-1}$) | Microporosity | | Mesoporosity | |
|---|---|---|---|---|---|---|
| | | | Area ($m^2$ $g^{-1}$)[a] | Volume ($N_2$)[1] ($cm^3$ $g^{-1}$) | Area ($m^2$ $g^{-1}$) | Volume ($cm^3$ $g^{-1}$) |
| Pt/AC | Fresh | 839 | 152 | 0.139 | 687 | 0.53 |
| | After reaction | 612 | 0 | 0 | 612 | 0.57 |
| Pt/CNF | Fresh | 114.6 | 13.6 | 0.007 | 100 | 0.25 |
| | After reaction | 111.5 | 11.4 | 0.005 | 101 | 0.26 |

[a] Obtained by the *t*-plot method.

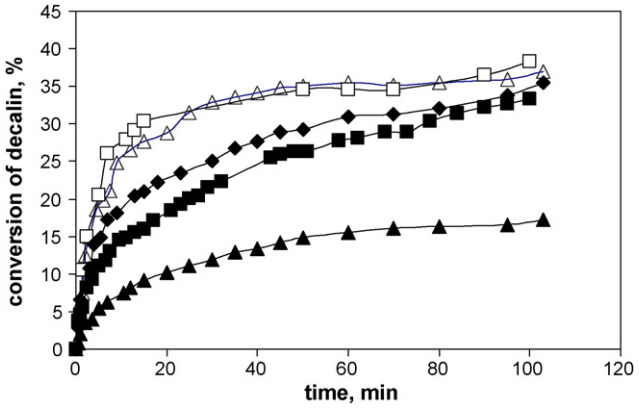


**Fig. 6.** Decalin conversion at 513 K as a function of time-on-stream for five different decalin/catalyst ratios performed with Pt/CNF catalyst (1.5 wt.% Pt). Volume of decalin to catalyst ratio (ml/g): (▲) 5; (■) 3.3; (◆) 2.7; (△) 2; (□) 1.

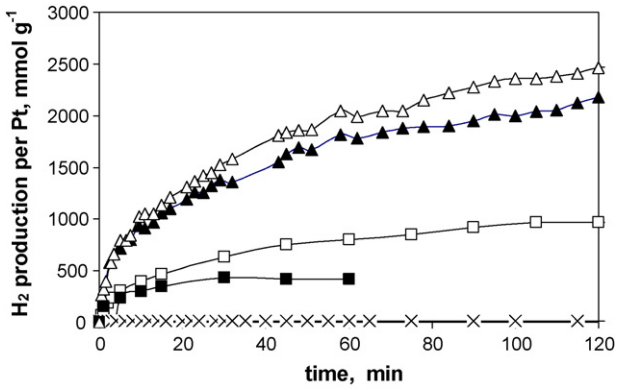


**Fig. 7.** $H_2$ production normalized by Pt weight (mmol $g^{-1}$) in the catalyst as a function of time on stream for the two catalysts: (△, ▲) Pt/CNF (1.5 wt.% Pt); (□, ■) Pt/AC (3 wt.% Pt); (×) blank experiments with CNF supports. Empty symbols correspond to the first use of the catalyst and filled symbols to the second use of the catalyst experimental conditions: reaction temperature = 513 K and decalin:catalyst ratio = 2.7 ml/g for both catalyst.

of conversion followed by an equilibration. This level off is mainly due to a decrease of reaction rate when approaching a thermodynamic equilibrium, although a partial deactivation of the catalyst by coke deposits cannot be disregarded. This deactivation has been evidenced because conversion diminishes in the second use of the catalyst (Fig. 7). The decalin/catalyst ratio is a very important parameter for process design. For the same conversion, the highest decalin/catalyst ratio is preferred because it maximises the amount of converted decalin, i.e. the $H_2$ volume produced in one pass. However, not all decalin/catalyst ratios led to the same conversion as it is observed in Fig. 6. With the highest decalin/catalyst ratio, i.e. 5 ml/g, the conversion attained is only 17%, which is the lowest conversion. This decline of conversion for high decalin/catalyst ratio is explained in the literature because the catalyst is flooded by the reactant. Thus, the optimal conditions leading to a thin superheated liquid film do not occur [6]. For the rest of the tested decalin/catalyst ratios, the final conversion is quite similar (around 35%) and close to the thermodynamic equilibrium (40% conversion) calculated in Section 3.1. However, more relevant than the final conversion is the conversion just after the steep conversion increase at the beginning of the experiment. This initial period of fast $H_2$ generation is interesting since we aim at using the catalyst in a car, where fast transients are needed. Furthermore, less deactivation of the catalyst is expected to take place in this first part of the curve. The highest initial conversion, around 30%, is met with two decalin catalyst ratios, namely 2 and 1 ml/g. Since 2 ml/g generates higher volume of $H_2$, this is the optimum decalin/catalyst ratio in our experimental system.

In the previous work with Pt/AC, the optimum decalin/catalyst was found between 2 and 2.7 ml/g. This value is not far from the value found for the Pt/CNF catalyst in this work, despite of ninefold lower surface area of Pt/CNF compared with Pt/AC, as shown in Table 2 and Fig. 8. Assuming that the optimum ratio is that leading to a thin reactant film over the catalyst surface, one would expect much lower optimum decalin/catalyst ratio for Pt/CNF than for Pt/AC.

Fig. 7 shows the specific $H_2$ production for experiments carried out using Pt supported on both carbon supports, i.e. Pt/AC and Pt/CNF. The conditions of the experiments were the same with both catalysts, i.e. 513 K and 2.7 decalin/catalyst ratio. This decalin/catalyst ratio led to the highest conversion with Pt/AC catalyst previously [17]. Both Pt/CNF and Pt/AC catalysts have different Pt loadings. Nevertheless, Pt is highly dispersed and with similar nanoparticle sizes in both catalysts as evidenced in Section 3.2. Despite the different Pt loadings, the normalization by platinum weight in Fig. 7 allows a visual comparison. It is apparent from Fig. 7 that the specific $H_2$ production is ca. fourfold higher for the Pt/CNF than for Pt/AC. Moreover, the decrease of $H_2$ production rate occurs slowly for Pt/CNF while $H_2$ production has already reached its maximum in a short time (ca. 50 min) for Pt/AC. This points out a faster deactivation in the case of the activated carbon-supported catalyst. Nevertheless, the activity decreases significantly in the second use of both catalysts.

To get some insight into the deactivation mechanism, we performed $N_2$ adsorption and CO chemisorption experiments with catalysts after reaction. Fig. 8 displays the $N_2$ adsorption isotherms and Table 2 displays the textural parameters for both Pt/AC and Pt/CNF before and after the catalytic tests. The porosity of Pt/AC encompasses both micro and mesopores while the porosity of Pt/CNF comprises mainly mesoporosity. Despite the much higher surface area and pore volume of Pt/AC, there is a complete closure of micropores after the catalytic test. This occurs most likely by carbonaceous deposits as shown in the literature [18]. Since the platinum catalyst is mainly located in micropores of Pt/AC, most Pt becomes inaccessible. The plugging is not observed in Pt/CNF because the absence of microporosity. Other cause different from pore plugging must account for deactivation in the case of Pt/CNF. CO chemisorption (Table 1) showed that metallic surface area

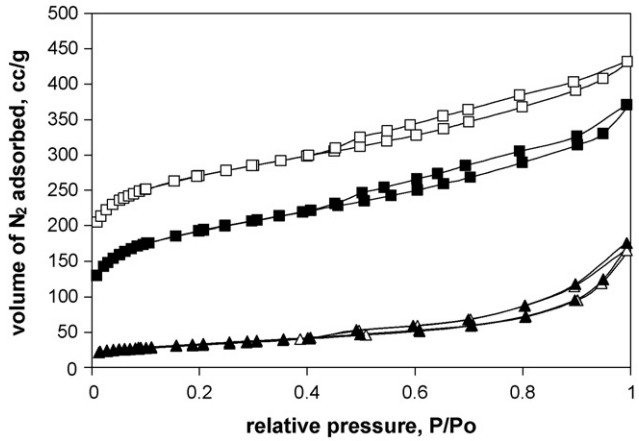


**Fig. 8.** $N_2$ adsorption isotherms (77 K) for Pt/CNF and Pt/AC catalyst before and after catalytic tests. Pt/CNF, (△) before reaction (▲) after reaction; Pt/AC, (□) before reaction (■) after reaction.

decreases only slightly for Pt/CNF. Therefore, sintering is not a major deactivating mechanism. Presumably, coke deposits can explain deactivation for Pt/CNF.

### 3.4. Use of monolithic reactor for process intensification

In the literature, dehydrogenation in gas phase of, e.g. methylcyclohexane has been carried out with different reactor configurations such as with wall-coated reactors [19] to enhance the heat transfer or membranes selective to $H_2$ [20] to enhance conversion. In the former case, the operation temperature used was higher than 400 °C and in the latter methylcyclohexane was diluted in an inert gas. It is not straightforward to extrapolate these reactor configurations to the reaction studied here, since decalin dehydrogenation must be carried out with concentrated reactant and at temperature lower than 400 °C to prevent coke deposition. Hence, there is the challenge of designing a reactor for dehydrogenation in continuous at low temperatures and feeding a concentrated liquid reactant. Several authors have recognised the benefits of carrying out the dehydrogenation in conditions of "liquid-film state" [6,7,12] or also called "wet–dry multiphase conditions" [3,11]. In this special contact between reactant and catalyst, the catalyst experiences alternating wet and dry conditions. This operation mode has advantages over both liquid and gas phase reactions. Over liquid phase reaction, the thin liquid-film is super-heated, thus favouring the endothermic reaction. Moreover, $H_2$ product diffuses to gas phase easily through the thin reactant liquid film without formation of bubbles and this $H_2$ evolution shifts the chemical equilibrium to dehydrogenation. Furthermore, also adsorbed aromatic products are removed during the drying step preventing site blocking, which is often observed in liquid phase reaction.

This unsteady wet–dry conditions are created in the literature by using a spray pulse reactor [3,4,13,21,22]. In this reactor, a nozzle feeds atomized liquid reactant in pulses, creating alternating wet and dry conditions on the heated solid catalyst surface where the catalyst is forming a thin catalyst layer deposited over a plate.

For the commercial feasibility of the process, the intensification of the process is crucial, taking into account that the available volume in a vehicle or portable device is very limited. As far as we know, using a monolithic catalytic reactor would increase the volume activity because monoliths have a high geometric surface area. Monoliths made out of metal will favour the heat transference necessary to sustain the endothermic reaction. In order to perform this reaction in alternating liquid-film and dry conditions we propose a reactor concept based on a rotating monolith like that patented by Moulijn and Edvinsson [23] for multiphase reactions. The rotating monolith has also been proposed for gas phase dehydrogenation to produce alkenes [24]. A schematic picture of the rotating monolith concept is displayed in Fig. 9. The surface of the monolith channels can be easily coated with the desired catalyst [25]. In addition, the preparation of monoliths coated with CNF has been widely documented [26–28]. In the rotating monolith reactor, the monolith rotates around a horizontal shaft and the catalyst in the channels is alternately in contact with the liquid phase and with the gas phase. Thus, the monolith would undergo alternating wet and dry conditions as those sought for in batch experiments and in the spray pulse reactor reported in the literature. The mode of operation is as follows. First, the monolith is wetted in decalin. When the monolith rotates, the part in contact with the liquid is progressively withdrawn from the liquid and it enters the dry section. The excess of liquid is drained from the monolith channels by a gravitational effect and a thin reactant liquid layer is retained over the catalyst surface. Thus, the monolith experiences dry conditions in which the dehydrogenation reaction takes place, releasing $H_2$ to the gas phase.

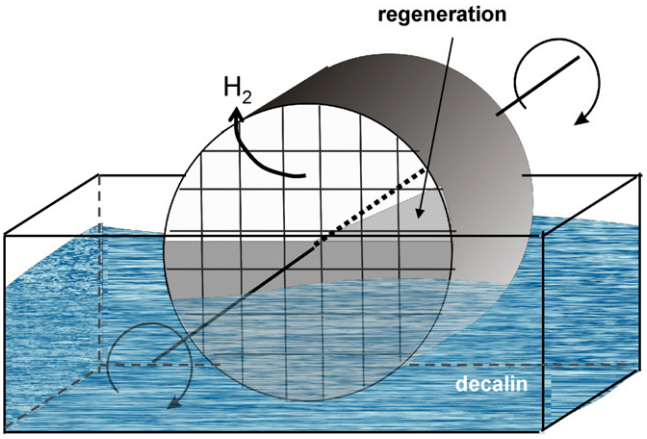


**Fig. 9.** Rotating monolith concept proposed for in situ $H_2$ production from decalin.

This concept also allows to take advantage of the high dehydrogenation rate at the beginning of the batch experiment (Fig. 6), avoiding the operation in the region of low activity where some deactivating species, as e.g. coke, might deposit over the catalyst. Even this reactor configuration would permit the introduction of optional regeneration steps (Fig. 9), as e.g. a mild oxidative treatment to remove coke.

The main drivers in the development of a rotating monolith reactor for this reaction may be summarised as follows:

- structured catalyst reactor,
- avoiding granular catalyst,
- high catalytic geometric surface area, maximising working volume,
- alternating wet and dry conditions and thin liquid film,
- exploitation of observed initial high catalyst activity avoiding operation in deactivating conditions, and
- possibility of introducing a regeneration step.

## 4. Conclusions

We have prepared a catalyst of Pt supported on carbon nanofibers with a good Pt dispersion, corresponding to a particle size around 2 nm. This catalyst has been tested in the dehydrogenation of decalin for in situ $H_2$ generation and it has been compared with a catalyst of Pt supported on a micro–mesoporous activated carbon. The catalyst supported on nanofibers exhibited fourfold higher $H_2$ specific productivity than the catalyst supported on activated carbon. This cannot be only attributed to Pt dispersion because both catalysts have comparable Pt crystallite size. In addition, the CNF-supported catalyst was less prone to deactivation because some deposits readily plugged the micropores of the activated carbon.

The decalin/catalyst ratio in the feed has a significant impact on the attained conversion. The highest decalin/catalyst ratio, i.e. 5 ml/g, led to a low conversion (17%) while lower decalin/catalyst ratios led to conversions around 35%, which is close to thermodynamic equilibrium. The optimum decalin/catalyst ratio, in terms of highest reaction rate, conversion and highest amount of decalin fed to the reactor, is met with a decalin/catalyst ratio of 2 ml/g. Finally, we have highlighted the potential advantages of monoliths as an alternative to other reactor configurations used in the literature for in situ $H_2$ generation in continuous.

## Acknowledgements

Spanish national research council (CSIC) is acknowledged for the financial support through "Proyecto Intramural" 200780/010. We appreciate very much the suggestions of the reviewers for improving this manuscript.

## References

[1] N.F. Grunenfelder, T. Schucan, Int. J. Hydrogen Energy 14 (1989) 579.
[2] E. Newson, T. Haueter, P. Hottinger, F. Von Roth, G.W.H. Scherer, T. Schucan, Int. J. Hydrogen Energy 23 (1998) 905.
[3] N. Kariya, A. Fukuoka, T. Utagawa, M. Sakuramoto, Y. Goto, M. Ichikawa, Appl. Catal. A: Gen. 247 (2003) 247.
[4] R.B. Biniwale, N. Kariya, H. Yamashiro, M. Ichikawa, J. Phys. Chem. B 110 (2006) 3189.
[5] D. Klvana, A. Touzani, J. Chaouki, G. Belanger, Int. J. Hydrogen Energy 16 (1991) 55.
[6] S. Hodoshima, H. Arai, S. Takaiwa, Y. Saito, Int. J. Hydrogen Energy 28 (2003) 1255.
[7] S. Hodoshima, S. Takaiwa, A. Shono, K. Satoh, Y. Saito, Appl. Catal. A: Gen. 283 (2005) 235.
[8] C. Shinohara, S. Kawakami, T. Moriga, H. Hayashi, S. Hodoshima, Y. Saito, S. Sugiyama, Appl. Catal. A: Gen. 266 (2004) 251.
[9] B. Wang, D.W. Goodman, G.F. Froment, J. Catal. 253 (2008) 229.
[10] E. Clot, O. Eisenstein, R.H. Crabtree, Chem. Commun. (2007) 2231.
[11] N. Kariya, A. Fukuoka, M. Ichikawa, Appl. Catal. A: Gen. 233 (2002) 91.
[12] S. Hodoshima, H. Arai, Y. Saito, Int. J. Hydrogen Energy 28 (2003) 197.
[13] R.B. Biniwale, N. Kariya, M. Ichikawa, Catal. Lett. 105 (2005) 83.
[14] Y. Wang, N. Shah, G.P. Huffman, Energy Fuels 18 (2004) 1429.
[15] Y. Wang, N. Shah, F.E. Huggins, G.P. Huffman, Energy Fuels 20 (2006) 2612.
[16] I. Suelves, M.J. Lazaro, R. Moliner, Y. Echegoyen, J.M. Palacios, Catal. Today 116 (2006) 271.
[17] D. Sebastian, E.G. Bordeje, L. Calvillo, M.J. Lazaro, R. Moliner, Int. J. Hydrogen Energy 33 (2008) 1329.
[18] R.K. Herz, W.D. Gillespie, E.E. Petersen, G.A. Somorjai, J. Catal. 67 (1981) 371.
[19] S. Tschudin, T. Shido, R. Prins, A. Wokaun, J. Catal. 181 (1999) 113.
[20] P. Ferreira-Aparicio, I. Rodriguez-Ramos, A. Guerrero-Ruiz, J. Catal. 212 (2002) 182.
[21] R.B. Biniwale, H. Yamashiro, M. Ichikawa, Catal. Lett. 102 (2005) 23.
[22] I. Kobayashi, K. Yamammoto, H. Kameyama, Chem. Eng. Sci. 54 (1999) 1319.
[23] R.K. Edvinsson, J.A. Moulijn, Patent no. WO 98/30323 (1998).
[24] E.H. Stitt, S.D. Jackson, D.G. Shipley, F. King, Catal. Today 69 (2001) 217.
[25] X.D. Xu, J.A. Moulijn, Stud. Surf. Sci. Catal. 118 (1998) 845.
[26] K.M. de Lathouder, D. Lozano-Castello, A. Linares-Solano, F. Kapteijn, J.A. Moulijn, Carbon 44 (2006) 3053.
[27] N. Jarrah, J. van Ommen, L. Lefferts, Catal. Today 79/80 (2003) 29.
[28] E. Garcia-Bordeje, I. Kvande, D. Chen, M. Ronning, Carbon 45 (2007) 1828.